ELSEVIER

Journal of Structural Geology 27 (2005) 1046–1060

JOURNAL OF STRUCTURAL GEOLOGY

www.elsevier.com/locate/jsg

Structural analysis of high-pressure shear zones (Bacariza Formation, Cabo Ortegal, NW Spain)

P. Puelles[a,*], K.F. Mulchrone[b], B. Ábalos[a], J.I. Gil Ibarguchi[c]

[a]*Department de Geodinámica, Universidad del País Vasco, P.O. Box 644, E-48080 Bilbao, Spain*
[b]*Department of Applied Mathematics, National University of Ireland, Cork, Republic of Ireland*
[c]*Department de Mineralogía y Petrología, Universidad del País Vasco, P.O. Box 644, E-48080 Bilbao, Spain*

Received 26 May 2004; received in revised form 9 March 2005; accepted 14 March 2005
Available online 4 June 2005

Abstract

High-pressure granulites of the Bacariza Formation (Cabo Ortegal Complex, NW Spain) exhibit spectacular examples of ductile shear zones developed at different scales in rocks containing pre-existing foliations. A detailed structural analysis was carried out on these shear zones in order to unravel and compare the role of various parameters controlling the deformation process (i.e. heterogeneous simple shear, components of homogeneous deformation, heterogeneous volume change and degree of non-coaxiality). Although heterogeneous simple shear largely dominated, negligible deviations from the ideal simple shear model were detected involving shortening along the structural directions perpendicular to the stretching axis (within the foliation plane) of the finite strain ellipsoid. The relationship between displacement parallel to a half-shear zone and the normal distance from its boundary provided the basis for the estimation of the stress exponent in the power-law constitutive flow equation associated with each shear zone, which is interpreted as a rheological indicator. These geometric and rheological results, and the thermobaric conditions of high-pressure shear zone deformation, indicate that these shear zones accommodated dominant plastic rock flow coeval with high-pressure and high-temperature deformations under moderate stress levels concomitant with elevated strain rates.

Keywords: Cabo Ortegal; High-pressure granulites; Shear zones; Deformation; Rheology

1. Introduction

The existence of ductile shear zones within a rock body is a manifestation of deformation localization. Shear zones often arise as mechanical instabilities governed by processes other than simple shear and exhibit self-similar geometrical patterns over a range of scales (Carreras, 2001). Ramsay and Graham (1970) and Ramsay (1980) used the concept of 'strain compatibility' and other geometric arguments to prove that ideal ductile shear zones develop under any combination of three main types of displacement fields: (1) heterogeneous simple shear, with the shear plane oriented parallel to the shear zone walls, (2) heterogeneous dilation, with a volume change associated with displacement perpendicular to the shear walls, and (3) homogeneous strain of any type affecting the shear zone and its wall rocks. In natural shear zones these three end-members are expected to combine in different proportions during or after shear zone development.

Mesoscopic ductile shear zones developed in high-pressure granulites under medium- to high-grade metamorphic conditions are described, analysed and interpreted in this study. A detailed structural analysis founded on classical geometrical arguments (Gapais et al., 1987; Ghosh and Sengupta, 1987; Ramsay and Huber, 1987; Jain, 1988; Mohanty and Ramsay, 1994) and a rheological analysis following the quantitative method proposed by Mulchrone (2001) after Talbot's (1999) model are used to determine the relative importance of each of the deformation components and also to gain insight into the behaviour of rocks in deep tectonic levels of an eo-Hercynian subduction zone (involving both continental crust and uppermost lithospheric mantle). Additionally, quantitative estimations of the stress regime operative during deformation is accomplished in

* Corresponding author. Tel.: +34 944648500; fax: +34 944648500
E-mail address: gpppuolp@lg.ehu.es (P. Puelles).

0191-8141/$ - see front matter © 2005 Elsevier Ltd. All rights reserved.
doi:10.1016/j.jsg.2005.03.002

order to contribute to a growing database of power-law exponents, which might allow the definition of quantitative deformation facies (Hansen, 1971; Tikoff and Fossen, 1999).

2. Geological setting

The Cabo Ortegal Complex is a composite nappe pile that forms part of the so-called Allochthonous Complexes of the northwestern Iberian Peninsula (Fig. 1a). These represent fragments of a subducted continental and oceanic lithosphere that were obducted onto the Gondwana edge during the Hercynian orogeny (Ries and Shackleton, 1971; Martínez Catalán et al., 1997). They are composed of various units metamorphosed under different high-pressure conditions and separated by thrust contacts. In Cabo Ortegal (Fig. 1b) a number of high-pressure nappe units can be mapped (ultramafic massifs, high-pressure granulites, N-MORB eclogite, metagabbro, metaserpentinite, metaperidotite and ortho- and paragneisses; cf. Vogel, 1967; Gil Ibarguchi et al., 2000, and references therein). One of them is the high-pressure granulite Bacariza Formation (Vogel, 1967; Galán and Marcos, 1997; Puelles, 2004).

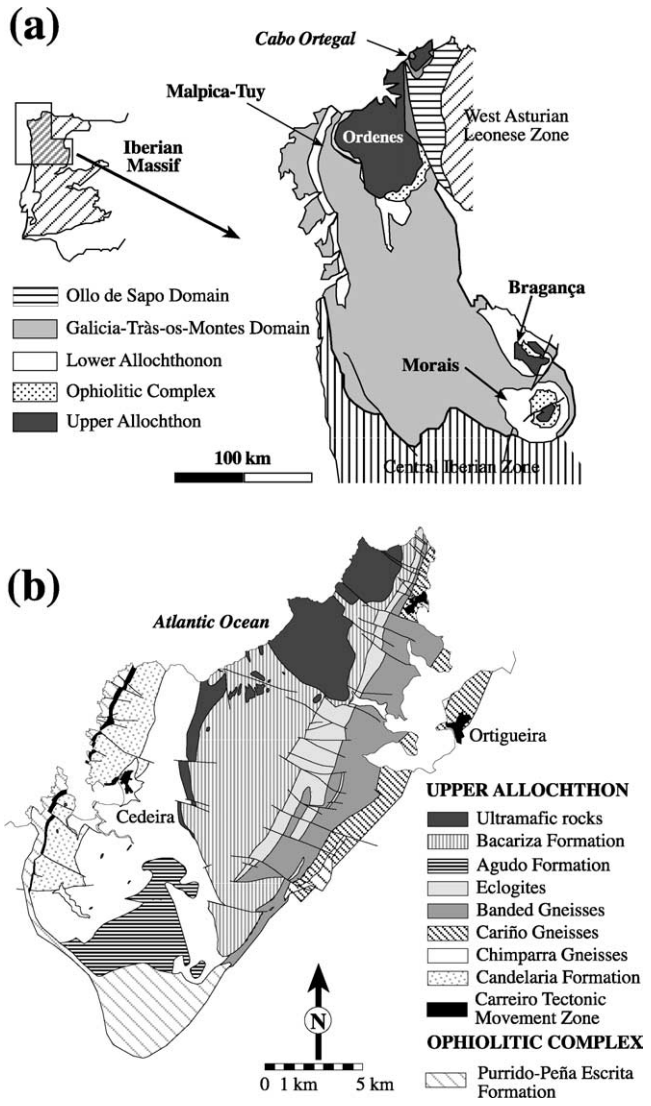

Fig. 1. (a) Geological sketch map of NW Iberia showing the units that constitute the Allochthonous Complexes and their para-autochthon (Domain of Galicia-Tràs-os-Montes). (b) Simplified geological map of the Cabo Ortegal Complex after Ábalos et al. (2000) showing the high-grade/high-temperature metamorphic nappe units (Upper Allochthon).

The primary structure of Cabo Ortegal rocks is related to early Variscan, high-pressure and high-temperature tectonic events (cf. Girardeau et al., 1989; Gil Ibarguchi et al., 1990, 2000; Girardeau and Gil Ibarguchi, 1991; Santos Zalduegui et al., 1996, 2002, 2002; Ordóñez et al., 2001). The ultramafic massifs rest on top of the high-pressure granulites of the Bacariza Formation, which overlie the eclogites, and finally high-pressure gneisses overlain by the eclogites. The contacts between these units have been described as ductile thrust contacts (Ábalos et al., 1996, 2003). Amphibolite-facies retrogression was estimated at ca. 380 Ma or slightly younger (Van Calsteren et al., 1979; Peucat et al., 1990; Santos Zalduegui et al., 1996), whereas greenschist-facies retrogradation was dated between ca. 350 and 360 Ma (Peucat et al., 1990; Dallmeyer et al., 1997).

3. The HP Bacariza Formation

The Bacariza Formation constitutes a heterogeneous formation dominated by garnet- and plagioclase-rich lithotypes. Granulites are mainly of basic (even ultramafic) to intermediate composition, although granitic, carbonatic, or mineralogically more exotic intercalations exist (Vogel, 1967; Gil Ibarguchi et al., 1990; Galán and Marcos, 1997; Puelles, 2004). The following granulite types can be differentiated (in order of decreasing abundance) after Puelles (2004): common mafic granulites or plagio-pyrigarnites (G1 in Fig. 2) that often alternate with intermediate to felsic plagioclase-rich granulites (G2), Mg-rich mafic granulites (G3), ultramafic granulites or pyrigarnites (G4) and granulitic orthogneisses (G5). Most of the granulite outcrops containing mesoscopic shear zones are found in intermediate to felsic (G2) and mafic (G2) granulites. They are characterized by a compositional and tectonic banding in which centimetre to metre thick mafic/ultramafic bands made of garnet, clinopyroxene and plagioclase (occasionally monomineralic bands of garnet or clinopyroxene) alternate with a similar proportion of light-coloured layers of intermediate composition made of plagioclase, quartz, and minor amounts of primary garnet, clinopyroxene and rutile. Felsic layers seemingly of in situ anatectic origin, enriched in mafic components along their edges are not uncommon in both the intermediate and mafic granulites.

Protolith radiometric ages for granulites are ca. 490 Ma (conventional and sensitive high-resolution ion microprobe

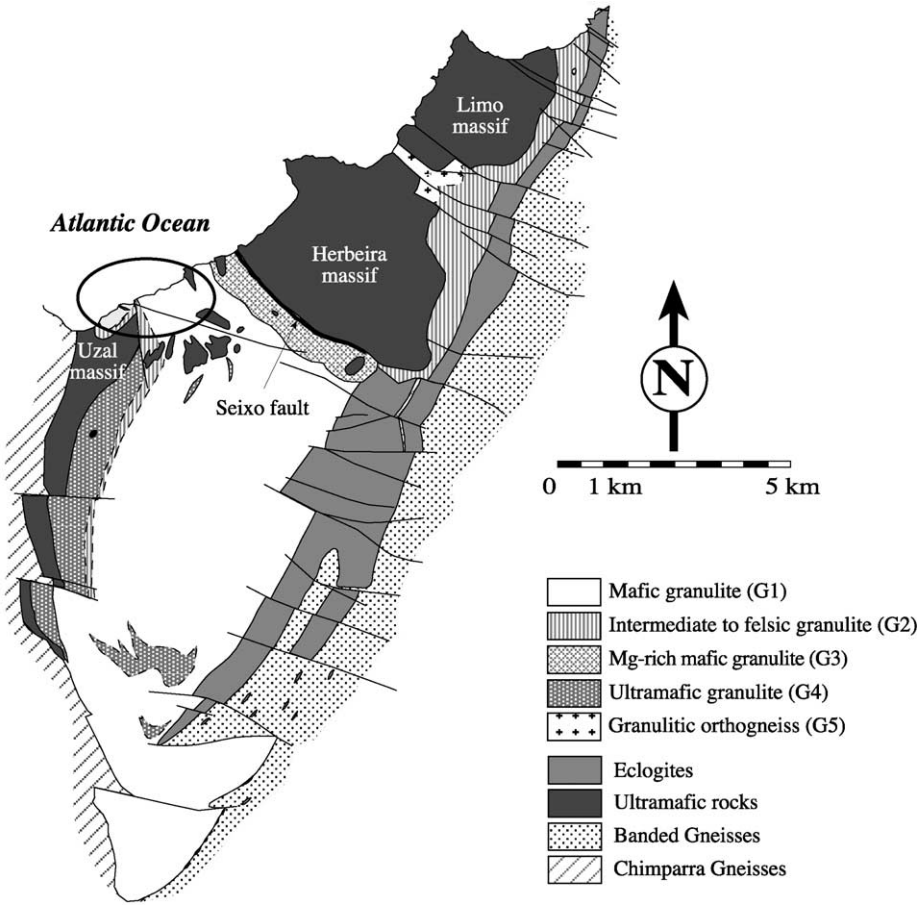

Fig. 2. Geological sketch map of the Bacariza Formation showing the different granulite lithotypes and bounding units. The ellipse indicates the location of the best exposed D2 shear zones.

SHRIMP U–Pb on zircon; Peucat et al., 1990; Ordóñez et al., 2001, respectively). Granulite facies metamorphism took place under conditions of up to 800 °C and >1.5 GPa (Gil Ibarguchi et al., 1987, 1990, 2000; Galán and Marcos, 2000; Puelles, 2004). U–Pb dating of titanite forming part of the high-pressure metamorphic mineral assemblage yielded ages of ca. 382–389 Ma (Santos Zalduegui et al., 1996).

4. Structural analysis of shear zones

Based upon microstructural and petrographic criteria, and on the nature and the geometrical relationship of both major and penetrative minor structures, a high-pressure deformational event can be recognized in the Bacariza Formation. In detail, this was a polyphase episode consisting of two phases of deformation termed D1 and D2.

4.1. D1 high-pressure deformations

D1 represents a complex progressive deformation. A principal planolinear fabric (S1–L1) is defined by the elongation and crystallographic preferred orientation of constituent high-pressure minerals. Garnet core or inner zone compositions with the highest Ca- or Mg-contents along with clinopyroxene cores with the highest jadeite and Fe have been selected in an aim to minimize the effect of late equilibria that might have affected the composition of the phases at the metamorphic peak. Accordingly, the most sodic compositions in inner portions of matrix primary plagioclases have also been selected. By combining individual spot analyses on the same thin section and simultaneously solving for the pressure and temperature conditions, the results obtained for the near-peak high-pressure granulite facies metamorphic event and the coeval D1 range from ca. 740 to 835 °C and 1.4 to 1.7 GPa with an average of 790 °C and 1.6 GPa (Puelles et al., in press) L1 is usually subhorizontal and trends NNE. Associated shear sense criteria indicate a top-to-the-NNE tectonic displacement of hanging wall blocks during D1 (Puelles et al., 2001; Puelles, 2004). Isoclinal D1 folds, on a decimetre to metre scale, commonly refold S1 and L1 and exhibit a sheath fold geometry. They deform and transpose the principal foliation and show geometries characterized by thickened hinges and thinned limbs in both *XZ* and *YZ* structural sections (i.e. *XY*, plane of foliation; *X*, mineral and stretching lineation direction). As fold axes are subparallel to the lineation L1 and fold axial surfaces are parallel to the regional foliation

S1, a genetic connection between S1/L1 and fold development is suggested. Eye- and anvil-like fold sections, typical of axis-perpendicular geometries of sheath folds, as well as Ramsay's (1967) type-3 fold interference patterns, have been identified in sections normal to L1 at the outcrop and map scales (Ábalos et al., 2003). These folds are occasionally associated with an axial planar foliation that might be described as a later fabric (i.e. S1b). However, since they are defined by the same high-pressure mineral assemblage as S1, this fabric is also considered as a D1 structure.

4.2. D2 high-pressure shear zones

During D2, localized deformation took place. S1–L1 and D1-fold structures were transposed in ductile shear zones and a new generation of planolinear and fold structures developed, as described below in further detail. D2 granulite shear zones, isoclinal and sheath folds, and associated mylonites show a close genetic relationship. Assuming that the measured mineral compositions in the strongly D2-deformed rocks may provide an approach to the physical conditions of the deformation, and following the P–T calculation criteria and routine described above, the values obtained for intermediate granulites (G2) close to the contact with the eclogites range from ca. 710 to 780 °C and 1.4 to 1.6 GPa, with an average of 740 °C and 1.4 GPa (Puelles et al., in press).

D2 shear zones are subparallel to the base of the overlying peridotite thrust (Figs. 2 and 3). At the map scale it can be observed that the basal contact of the peridotite allochthon cuts the S1 granulite foliation at a high angle. This can be also unravelled in 'down plunge' structural projections of the principal lithostratigraphic contacts and S1 foliation trajectories, as shown in Fig. 3. D2 shear zones and S2 foliation traces appear in Fig. 3 with subhorizontal attitudes parallel to the peridotite sole thrust. The thickness of each shear zone is often <30 cm (Fig. 4), though locally it may be several metres.

Within these shear zones, high-pressure S1 foliations are deformed and transposed into new cross-cutting S2 foliations (Fig. 4) that are defined by a mineral assemblage similar to that of S1. The majority of the shear zones are subhorizontal, displaying S2 foliations with a mean orientation of 15°/095°. The associated L2 stretching lineations plunge ca. 10°/025° (Fig. 5). The kinematics of D2 shear zones indicate a top-to-the-NNE tectonic displacement of hanging wall blocks.

Three mylonitic lithologies are locally found in close association with the shear zones forming planar blankets up to 1 m thick. These are: (1) very fine-grained, apparently structureless ultramylonitic rocks of fluidal appearance (Puelles, 2004), (2) garnet–clinopyroxene-bearing metacarbonate rocks (Gil Ibarguchi et al., 1987; Santos Zalduegui et al., 1996), and (3) garnet–biotite-rich intercalations, usually migmatitic, with restitic parts containing abundant garnet ± biotite and, occasionally, relic clinopyroxene in amphibole. Calculated thermobaric conditions for recrystallization of these rocks are ca. 705 °C and 1.1 GPa.

4.3. Deformation components in D2 shear zones

The results of a detailed analysis of D2 shear zone geometry are presented in the following sections. Influence of the variables that control shear zone development (proportions of homogeneous deformation, heterogeneous volume change and simple shear) during structural development is discussed with them. As far as homogeneous deformation (which affected both the shear zone and wall rocks together) is concerned, it is noted that the wall rocks of the shear zones are composed of strongly foliated and lineated high-pressure granulites pervasively deformed during D1. The orientation of S1 outside shear zones is maintained without inflections and there are no structures

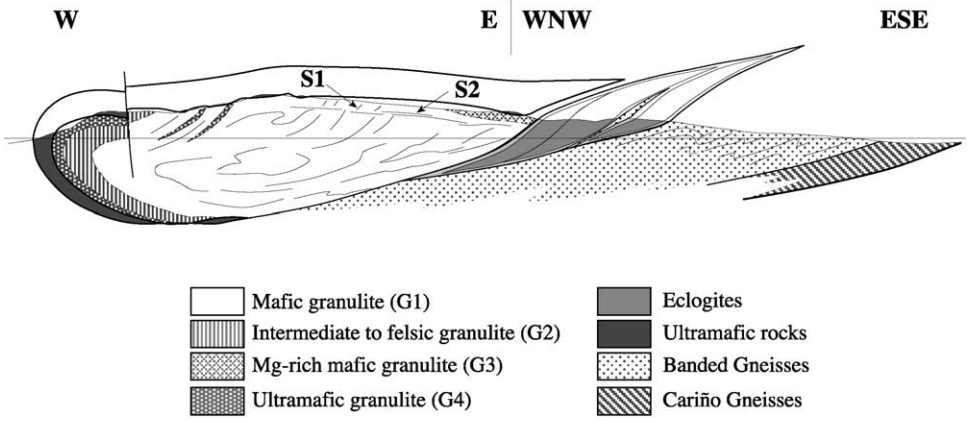

Fig. 3. Geological cross-section of the central sector of the Cabo Ortegal Complex showing the structural relationship between ultramafic rocks, high-pressure granulites (Bacariza Formation), eclogites and high-pressure gneisses. The cross-section corresponds to a plane perpendicular to the high-pressure mineral lineations. Note how the basal contact of the peridotite allochthon cuts the S1 granulite foliation at a high angle and how D2 shear zones and S2 foliation traces appear with subhorizontal attitudes parallel to the peridotite sole thrust.

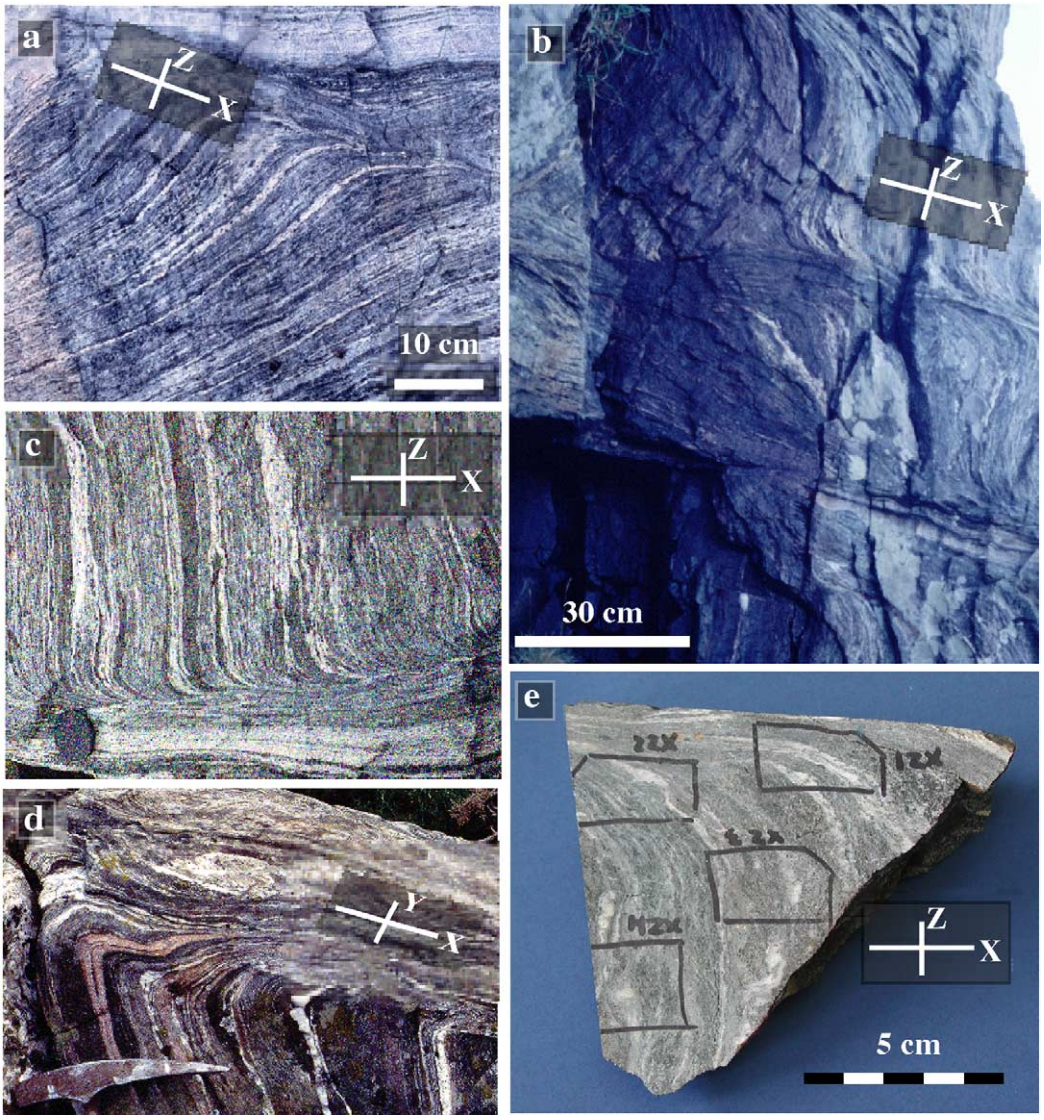

Fig. 4. (a)–(d) Field photographs of D2 shear zones deforming the S1 granulitic foliation in intermediate-felsic (G2) granulites. The outcrop surfaces are close to the plane normal to the shear zones and parallel to the stretching lineation. (e) Hand-specimen of a ductile shear zone where the microstructural transitions and the mineralogical composition of the mineral assemblage in equilibrium have been studied in different portions.

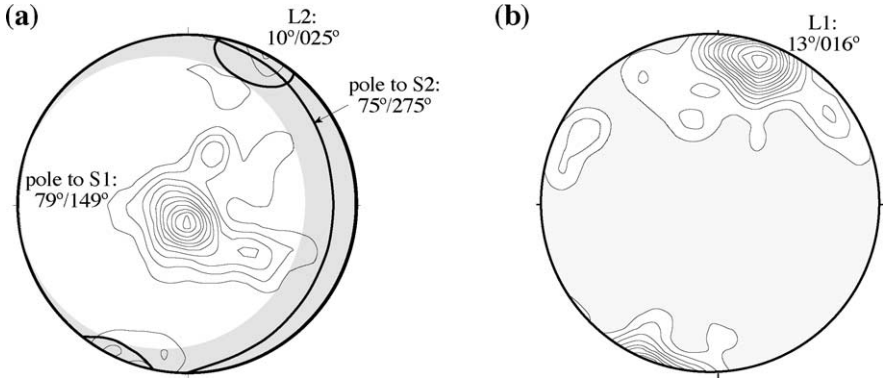

Fig. 5. (a) Equal-area projection showing the principal orientations of the S1 HP granulite facies foliation and the mean orientation depicted by the S2 foliations and L2 lineations measured in D2 shear zones (orientation of S1 and S2 given as the attitude of the pole to foliation). The shadowed area corresponds to the 15° confidence cone. (b) Equal-area projection showing the principal orientations of the L1 lineation.

indicative of deformation during D2 there. Shear zones display variable orientations with respect to the S1, which is strongly reoriented inside them. Thus, it can be reasonably assumed that the planolinear S1–L1 fabric was deformed only inside the shear zones during D2, and that the wall rocks either persisted undeformed or maintained a high competency contrast with the shear zones. Accordingly, since the component of superimposed D2 homogeneous deformation was probably negligible, heterogeneous volume change and/or heterogeneous simple shear are interpreted to be the most influential components of deformation.

Mohanty and Ramsay (1994) studied natural shear zone strain partitioning in the context of a two-dimensional plane strain kinematic framework. They proposed a geometric procedure to calculate volume change and simple shear components of shear deformation. Their method uses either the angles formed by two planar markers of different orientation both inside and outside the shear zone or the angles between shear zones, planar markers and the principal axes of the two-dimensional deformation ellipse. Since the D2 shear zones considered here have only one passive marker (i.e. S1, see Fig. 4), it was not possible to estimate the magnitude of volume change based upon the methods of Mohanty and Ramsay (1994). An alternative approach to volume change estimation is based on mineral chemistry variations across shear zones. Such variations have been related to the intensity of shear deformation and volume changes in shear zones (Beach, 1976; Mohanty and Ramsay, 1994; Valín et al., 1994; Ring, 1998, 1999; Sturm, 2003, and references therein), though other constraints can exist (Arbaret et al., 2001; Bhattacharyya and Hudleston, 2001). Petrographic studies and chemical–mineralogical analyses carried out in D2 shear zones reveal that the composition of the primary mineral phases and assemblages (Table 1) and the modal proportions of the minerals remain constant both in the interior and outside the shear zones (Puelles, 2004). Taking all this into account, heterogeneous volume change during D2 shear zone development is interpreted here to be negligible.

Mandal et al. (2001) presented a theoretical model (based upon energetic and thermodynamic grounds) to evaluate the degree of non-coaxiality in shear zones with rigid and deformable walls under constant volume conditions. According to these authors, the magnitude of flattening in shear zones is likely to be affected by (1) their length/width ratio, (2) the viscosity contrast between the wall rock and the shear zone, and (3) by the orientation of the shear zones with respect to the principal axes of bulk strain. On one hand, in shear zones showing a high length to width ratio, the flattening component are predicted to be negligible because their behaviour is close to that of heterogeneous simple shear. On the other hand, in shear zones with lower length to width ratios, the flattening component might be important. As regards viscosity contrasts, narrow shear zones hosted in more rigid wall rocks should be ideally dominated by heterogeneous simple shear deformations, whereas under low viscosity contrast conditions the flattening component might be important. Finally, when the angle between the direction of the tectonic displacement and the shear zone is small, rotational components of deformation are expected to be significant. In the Bacariza Formation, although only parts of the full length of the shear zones were accessible to observation (their whole length is much larger than the outcrop surfaces), they exhibit relatively high length to width ratios (systematically larger than 8–10), a high competency contrast between wall rocks and the shear zones and small angles with the likely direction of the tectonic displacement. Thus, according to the criteria cited above, flattening components can be considered negligible also and the deformation pattern for the ductile shear zones should approach heterogeneous simple shear.

Mulchrone (2004) has demonstrated that the mechanical basis of the model of Mandal et al. (2001) is flawed and that the results of this analysis should be discounted. Mandal et al. (2004), in reply to his comment, have simply underlined their failure to appreciate some basic physical constraints and principles that must be applied to all continuum mechanical models. As the final resolution of this issue is not the primary focus of the current paper, an alternative approach to the recognition of flattening of the type postulated by Mandal et al. (2001) in shear zones is introduced. Rather than attempting to evaluate an energy balance, displacement fields predicted to occur flattening shear zones are compared with naturally occurring displacement fields.

The flattening component of deformation is given by the cream cake model of Jaeger (1969, pp. 140–143) and Ramsay and Lisle (2000, pp. 998–999) with the following velocity field:

$$v_x = \frac{3v_b x(h^2 - x^2)}{2h^3} \qquad v_y = \frac{v_b y(y^2 - 3h^2)}{2h^3} \tag{1}$$

where v_x is velocity in the x-direction, v_y is velocity in the y-direction, $2h$ is the shear zone thickness, v_b is velocity of the shear zone boundaries in the y-direction and (x, y) gives the position at which the velocity occurs (see Fig. 6). Clearly as

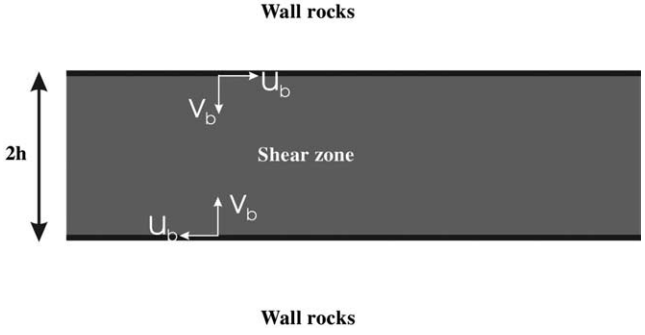

Fig. 6. Sketch showing the significance of the parameters involved in the resolution of the linear shear flow Eq. (5).

Table 1
Representative analyses of clinopyroxene (Cpx), garnet (Grt) and amphibole (Am) inside (in) and outside (out) the shear zone

Sample analysis	SZa.XZ; Cpx-7; Cpx-in	SZb.XZ4; Cpx-8; Cpx-out	Sample analysis	SZa.XZ; Grt-15; Grt-in	SZb.XZ4; Grt-30; Grt-out	Sample analysis	SZa.XZ; Am-2; Am-in	SZb.XZ4; Am-654; Am-out
SiO_2	50.60	51.02	SiO_2	39.12	38.73	SiO_2	43.05	42.56
TiO_2	0.45	0.34	TiO_2	0.04	0.07	TiO_2	1.16	1.23
Al_2O_3	7.11	7.04	Al_2O_3	21.84	21.65	Al_2O_3	13.74	12.98
Cr_2O_3	0.07	0.04	Cr_2O_3	bd	bd	Cr_2O_3	bd	bd
FeOt	6.62	8.62	FeOt	21.98	23.76	FeOt	13.05	14.90
MgO	11.54	10.07	MgO	7.5	6.26	MgO	11.89	10.99
MnO	0.06	0.10	MnO	0.62	0.69	MnO	0.13	0.09
CaO	20.86	19.74	CaO	9.82	9.59	CaO	12.08	12.19
Na_2O	2.19	2.58	Na_2O	bd	bd	Na_2O	1.75	1.77
K_2O	0.33	0.15	K_2O	bd	bd	K_2O	1.09	1.79
Total	99.82	99.70	Total	100.92	100.73	Total	97.92	98.52
Si	1.854	1.885	Si	2.966	2.969	Si	6.317	6.317
Al.IV	0.146	0.115	Al.IV	0.034	0.031	Al.IV	1.683	1.693
Al.VI	0.161	0.192	Al.VI	1.919	1.926	Al.VI	0.693	0.588
Ti	0.012	0.010	Ti	0.003	0.004	Ti	0.128	0.137
Cr	0.002	0.001	Cr	–	–	Cr	–	–
Fe^{3+}	0.130	0.094	Fe^{3+}	0.079	0.070	Fe^{3+}	0.158	0.059
Fe^{2+}	0.073	0.172	Fe^{2+}	1.315	1.453	Fe^{2+}	1.444	1.790
Mg	0.630	0.554	Mg	0.848	0.715	Mg	2.600	2.431
Mn	0.002	0.003	Mn	0.040	0.045	Mn	0.016	0.012
Ca	0.819	0.782	Ca	0.798	0.787	Ca	1.899	1.938
K	0.015	0.007	K	–	–	K(A)	0.203	0.338
Na	0.156	0.185	Na	–	–	Na(M4)	0.062	0.045
						Na(A)	0.435	0.469

Fe^{3+}/Fe^{2+} estimated by regression techniques and charge balance criteria (cf. Droop, 1987; Dale et al., 2000) assuming: 4 cations and 6 O (pyroxene), 8 cations and 12 O (garnet) and 23 O (amphibole); bd, below detection limits.

the shear zone boundaries come closer together the value of h becomes smaller. If the initial thickness of the shear zone is denoted by h_0 then $h = h_0 - v_b t$, where t is time. Substituting this result and the fact that:

$$v_x = \frac{\partial x}{\partial t} \quad v_y = \frac{\partial y}{\partial t} \tag{2}$$

into Eq. (1), the following system of non-linear ordinary differential equations for particle position (x, y) as a function of time is derived:

$$\frac{\partial x}{\partial t} = \frac{3v_b x((h_0 - v_b t)^2 - y^2)}{2(h_0 - v_b t)^3}$$
$$\frac{\partial y}{\partial t} = \frac{v_b y(y^2 - 3(h_0 - v_b t)^2)}{2(h_0 - v_b t)^3} \tag{3}$$

Additionally, the flow due to the relative motion of the shear zone walls must be taken into account. A linear shear flow profile is the only physically possible model for Newtonian fluids (Fletcher, 2001; Sonder, 2001), which is given by:

$$\frac{\partial x}{\partial t} = \frac{u_b}{h} y = \frac{u_b}{h_0 - v_b t} y \quad \frac{\partial y}{\partial t} = 0 \tag{4}$$

where u_b is the velocity in the y-direction at the upper shear zone boundary (see Fig. 6). The final equation to be solved is

$$\frac{\partial x}{\partial t} = \frac{3v_b x((h_0 - v_b t)^2 - y^2)}{2(h_0 - v_b t)^3} + \frac{u_b}{h_0 - v_b t} y$$
$$\frac{\partial y}{\partial t} = \frac{v_b y(y^2 - 3(h_0 - v_b t)^2)}{2(h_0 - v_b t)^3} \tag{5}$$

This is a highly non-linear system with no analytical solutions and therefore must be numerically solved.

Eq. (5) was solved using the NDSolve function of Mathematica and simple grid representations were generated using its graphics capabilities. Example solutions are shown in Fig. 7 for three u_b/v_b ratios (i.e. low—flattening dominated, medium—equal contributions and high—simple shear dominated) at different stages of shear zone evolution. It is clear from these solutions that even a minor component of flattening distorts the grid in such a way that opposing senses of shear occur at the shear zone walls. This is due to the parabolic flow profile in opposite senses generated by the flattening component. Since reversing of shear sense along shear zone walls has not been observed in the field we conclude that flattening did not play an important role in the evolution of the ductile shear zones studied. In addition, these models illustrate that variations in intensity of deformation should occur along strike of a flattened shear zone, which is a feature that has not been observed either.

It is interesting to consider the vorticity pattern generated in a shear zone consisting of both simple shear and flattening

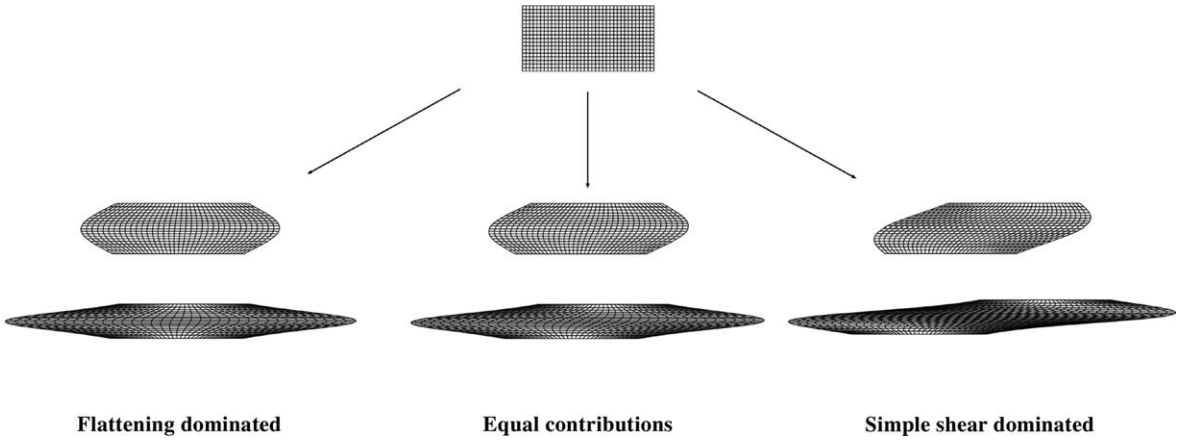

Fig. 7. Simple grid representation of Eq. (5) for low u_b/v_b ratios (flattening dominated), medium u_b/v_b ratios (equal contributions of flattening and simple shear) and high u_b/v_b ratios (simple shear dominated) at different stages of evolution.

for comparative purposes. As shown by Ghosh (1987) the kinematical vorticity number (W_k) can be calculated in terms of the velocity gradient tensor (L_{ij}) where:

$$L_{ij} = \frac{\partial v_i}{\partial x_j} \quad W_k = \frac{L_{12} - L_{21}}{\sqrt{(L_{12} + L_{21})^2 - 4L_{11}L_{22}}} \tag{6}$$

and in terms of the notation in Eqs. (1)–(5):

$$L_{11} = \frac{\partial v_x}{\partial x}; \quad L_{12} = \frac{\partial v_x}{\partial y}; \quad L_{21} = \frac{\partial v_y}{\partial x}; \quad L_{22} = \frac{\partial v_y}{\partial y} \tag{7}$$

so that for the flattening shear zone under consideration:

$$W_k = \frac{h^2 u_b - 3v_b xy}{\sqrt{h^4(u_b^2 + 9v_b^2) - 6h^2 v_b y(u_b x + 3v_b y) + 9v_b^2 y^2(x^2 + y^2)}} \tag{8}$$

Vorticity patterns are illustrated in Fig. 8 for the three cases studied. Again this diagram illustrates that for the presence of flattening there is change of sign of W_k across and along the shear zone.

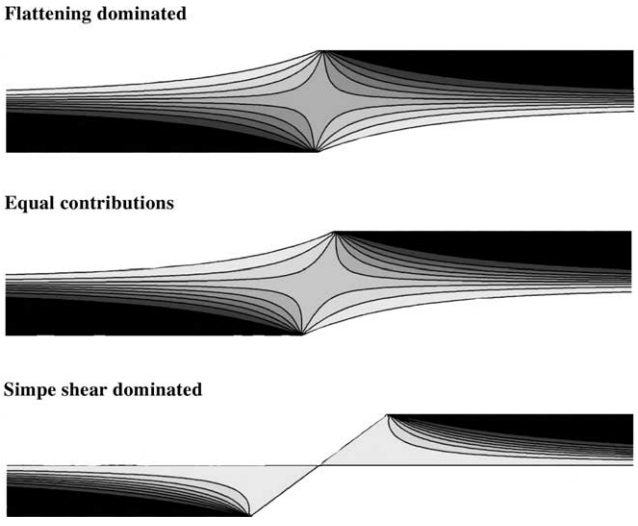

Fig. 8. Vorticity patterns generated in a shear zone consisting of both simple shear and flattening. Note that black colour indicates $W_k = -1$ (sinistral simple shear), white $W_k = 1$ (dextral simple shear) and shades of grey are at 0.2 intervals.

4.4. Shortening components normal to the direction of shear

The presence of a mineral and stretching lineation indicates stretching along the *X*-structural direction. Complementary to this, the close relationship between shear zones and similar folds, or even eye-like fold sections with axial surfaces parallel to the foliation in *YZ* structural sections (as well as in *XZ* sections), apparently reveals the existence of components of shortening parallel to the *Y* and *Z* principal strain axes, in spite of the fact that folds in shear zones can correspond to amplified and tightened perturbations (Carreras et al., 1977; Skjernaa, 1989; Alsop, 1992). Consequently, the bulk deformation ellipsoid related to D2 shear zones should in principle be classified as an ellipsoid of general constriction (Ramsay and Huber, 1983). Whereas this would be in agreement with many strain measurements in rocks (e.g. Hossack, 1968; Hudleston and Schwerdtner, 1997) suggesting that the state of natural strain is rarely of 'plane strain' type, such a constrictional ellipsoid representing non-plane strains is in principle contradictory with the arguments given above stating the predominance of heterogeneous simple shear deformation and plane strain.

Taking into account that the strain geometry actually observed in D2 shear zones does not record quantitative evidence of the undeformed state, it would be projected in the field for apparent constriction of Flinn's (1962) diagram. In this diagram, plane strain marks the frontier between the constriction and flattening fields and in the presence of components of positive volume change (dilation) the location of this boundary is displaced in such a way that (1) ellipsoids projected in the field of apparent constriction can represent general constriction, true plane strain and even flattening deformation. This can provide a basis for resolving the apparent contradiction between the results of the geometrical analysis of D2 shear zones and the

observation of fold structures in structural sections normal to the lineation, though this does not explain the reason why such fold structures actually occur. This question will be discussed later in further detail.

4.5. Geometry of D2 shear zones: isogon analysis

Assuming a plane strain deformation context for D2 shear zones, a quantitative study of their geometry using the classical technique of isogon analysis (Carreras and García-Celma, 1982; Ramsay and Huber, 1983; Carreras, 2001) makes sense in order to investigate the effects of deformation on alternate rock layers of different viscosity. This analysis also enables quantification of shear strain magnitudes and tectonic displacements. To this end, pre-existing S1 foliations and the thickness of the compositional banding were used as strain markers in the D2 shear zones (Fig. 9).

Compositional layer thickness measured normal to the foliation decreases towards the inner parts of shear zones. However, if measured parallel to the shear zone direction, they remain stable or, more commonly, increase. This variation in layer thickness is not homogeneous, which is particularly evident in mafic layers. However, layers rich in felsic components may show a decrease in thickness parallel to the shear zone.

Consideration of isogons attitudes within the shear zones (Fig. 9) shows that they define zigzag-like trajectories, reflecting the control exerted by the more competent layers (of more mafic composition) on strain geometry. Isogons exhibit a clear tendency to converge towards the inner parts of shear zones, reflecting increasing deformation gradients and strain.

4.6. Quantification of shear strain

Passive rotation of S1 foliation traces deformed by heterogeneous simple shear gives rise to special geometrical relationships in the profile section of a shear zone (i.e. in the section normal to the shear zone that contains the shear direction). In such a plane, the angle α between an undeformed linear marker of the shear zone walls and the shear zone direction is modified to α' after simple shear deformation of magnitude γ within the shear zone. These quantities are related by a simple equation (Ramsay and Graham, 1970) that permits the calculation of γ from α and α' angles measured from profiles of natural shear zones:

$$\cot \alpha' = \cot \alpha + \gamma \tag{9}$$

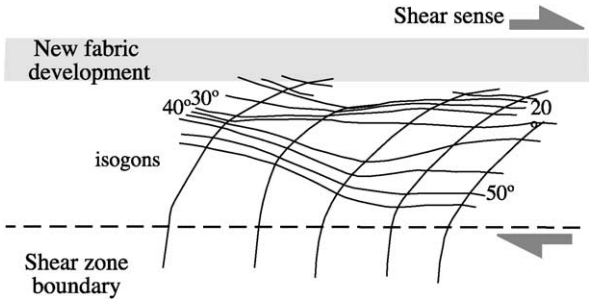

Fig. 9. Explicative sketch of the symbols and nomenclature used for shear zones. The absence of layer and fabric distortion has been used to define the boundary between wall rocks and shear zones. The inner boundary corresponds to the location where a new continuous fabric develops. The angle α is defined as the angle between the wall rock fabric and the shear zone. In order to measure α' (angle between the deflected layers and the shear zone) isogons have been traced at 5° intervals.

Digital images of exposures of D2 shear zones were collected from sections parallel or subparallel to the plane that is normal to the shear plane and parallel to the stretching lineation. Using these images, deflected layers (strain markers) were traced and geometrically analysed (Figs. 9 and 10). The boundary between wall rocks and shear zones was established by the absence of layer and fabric trajectory distortions. The α angles between the wall rock fabric trajectories and the shear zone boundary could then be readily measured. In order to determine equivalent angles inside the shear zones (α'), isogons were traced at 5° intervals (Fig. 9) and superimposed on the fabric trajectories (Fig. 10a–g). The innermost boundary of the deflected layers used for measurements was taken to be the location where a new penetrative fabric (S2) developed. As already stated, the central parts of the shear zones contain a new fabric oriented nearly parallel to their boundaries (Fig. 9) which transposes the S1 fabrics in the walls.

The lengths of isogon segments between the 5° intervals of the reference surfaces were measured and their normalized values (with respect to the total length of the linear markers) were used to plot them versus the respective angles α' (Fig. 10f–j). In these diagrams, the curves represented exhibit stair-stepped geometries with small slope plateaus located in zones ca. 10° wide located at positions where the α' angles vary principally between 10 and 20°. In some shear zones, these special features occur in the 30–40° interval of α' (Fig. 10 h) or paired in the 15–30 and 35–55° intervals (Fig. 10f and i). The 0–10° α' interval of all these diagrams corresponds to the portions of the shear zones where the deflected markers are transposed by a new S2 fabric. This angle is slightly greater in the shear zone SZ4 (Fig. 10d and i) and notably different in the shear zone SZ3 (Fig. 10c and h).

In Fig. 11, contours for shear strain γ are represented using Eq. (9) viz. α and α'. The inset area in Fig. 11a is zoomed in Fig. 11b, where a larger set of γ curves is presented for reference and used as a template for plotting the α–α' spaces associated with the shear zones analysed in Fig. 10. In this diagram, α–α' spaces (range of variation of strain marker orientations within the shear zones with error intervals of $\pm 5°$) are drawn as solid bars with arrows that point to the region where the angles between the deformed markers and the shear zones become smaller. The magnitude of shear strain (γ) that can be determined from

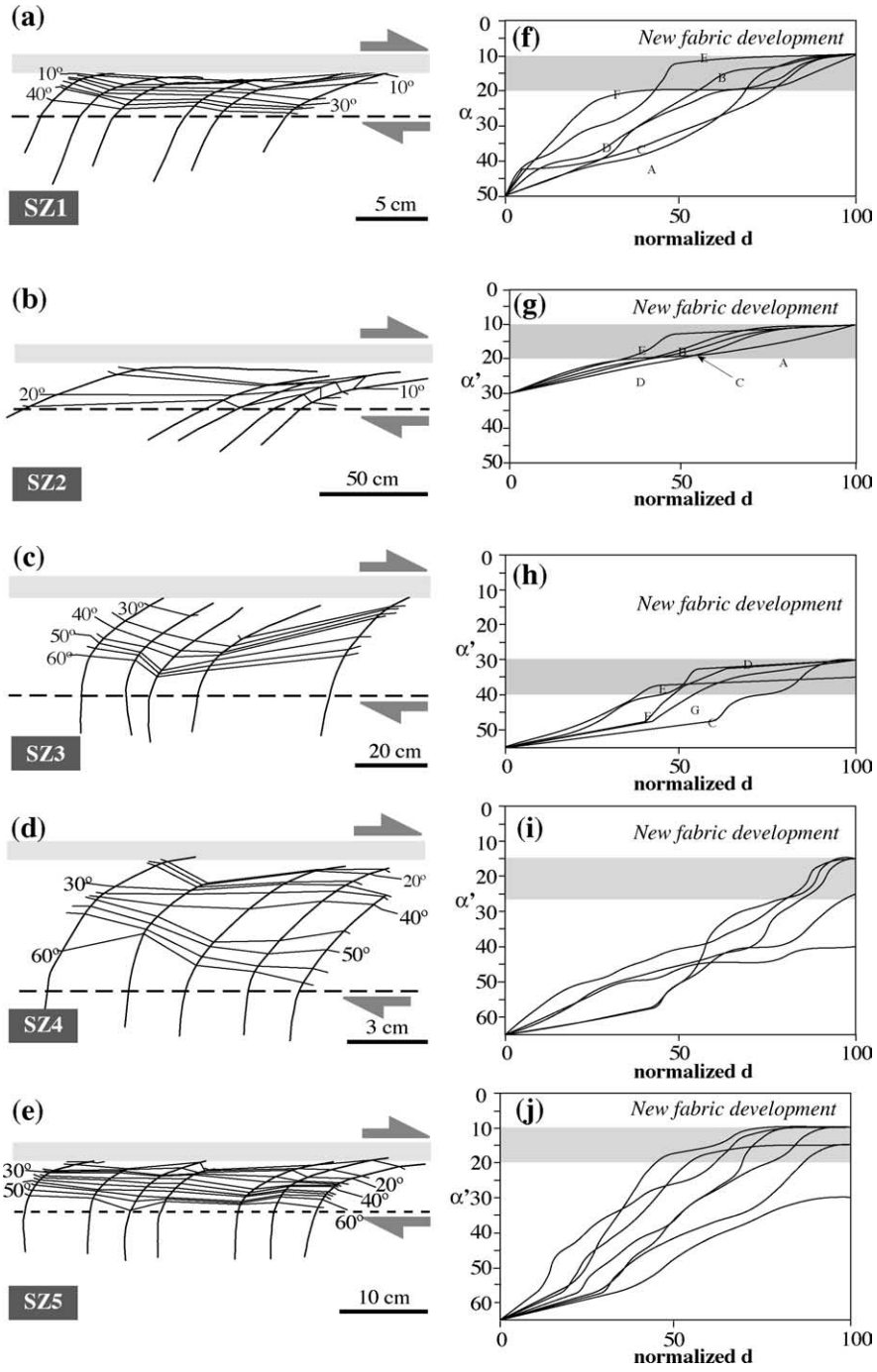

Fig. 10. (a)–(e) Style of five representative D2 shear zones defined by reference surfaces (S1 foliations drawn from field photographs in black). Geometrical analysis based on the construction of dip isogons (thin lines with numbers indicating the angle made with the strike of the shear zone). (f)–(j) Calculated plots showing the normalized proportion of the reference lines versus the angle α' made with the shear zone. Note that the curves show stair-stepped geometries with small slope plateaus.

this analysis ranges from 1 to 9, the maximum values being 5–9. This suggests that the portions of the shear zones where the S1 foliations are passively deformed accommodated lateral displacements of the order of 10 times their thickness (i.e. metre to decametre displacements). The shear strain within the innermost parts of the shear zones is probably of a much higher magnitude and, irrespective of the initial orientation of the markers, led to the development of a new tectonic fabric S2. This suggests that the total displacement across each of the D2 shear zones is probably much greater than that exhibited by deformation of S1 alone (i.e. $\gamma > 5$–9) and since the shear zones are stacked in vertical structural sections, the displacements add up within the Bacariza Formation. As a whole, the portion of the Bacariza

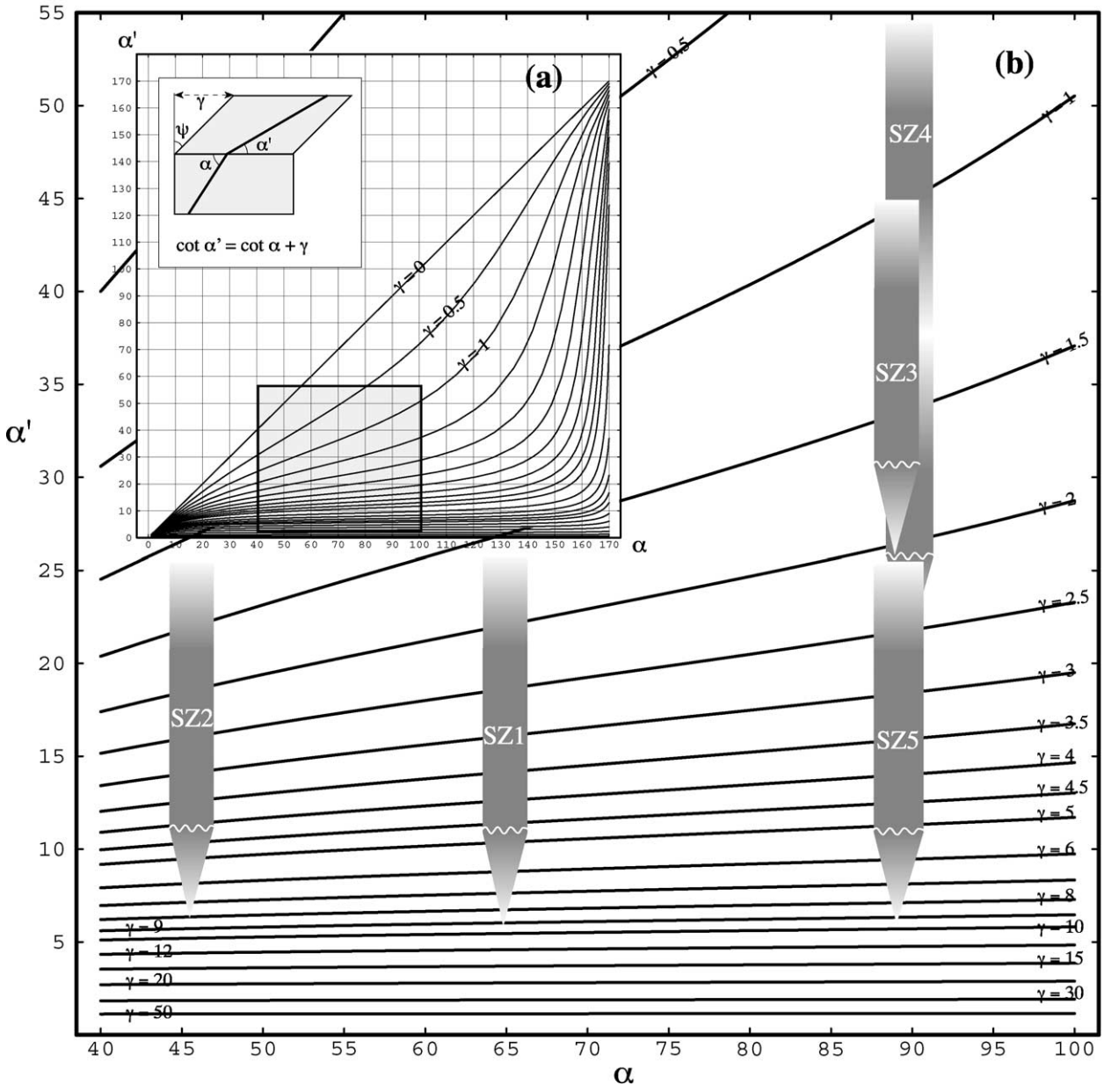

Fig. 11. (a) Plot of the function cot $\alpha' = \cot \alpha + \gamma$ for α- and γ-values in the ranges 0–180° and 0–100, respectively. The shear strain $\gamma = \tan \psi$ is indicated in the upper-left square in the figure. The shadowed square in the lower part is enlarged in (b). (b) Enlarged portion of Fig. 8(a) showing the angular relations for the studied shear zones and the calculated magnitude of the shear strain.

Formation studied is situated close to the basal contact with the ultramafic massifs and therefore, has probably accommodated tectonic displacements of the order of kilometres.

5. Rheological analysis on D2 shear zones

Stress–strain relationships are mathematically expressed by means of constitutive equations (or flow laws; cf. Nicolas and Poirier, 1976; Harris, 1977; Means, 1990) of the type:

$$\dot{e} = A\sigma^n \exp(-E^*/\mathrm{RT}) \quad (10)$$

where $\dot{e}$ is the strain rate (s^{-1}), A is an empirical constant ranging (for many rocks) between 100 and 500 kJ mol^{-1}, n is the stress exponent (ranging between 1 and 5 depending upon the specific rheological behaviour), E^* is the activation energy (kJ), R is the gas constant and T is the absolute temperature. The value of the parameter n determines whether the rheology of a given material is linear (e.g. viscous, with $n=1$), power-law or exponential (e.g. plastic). Materials in which $n \neq 1$ denote deviations from ideal viscous behaviour. For plastic behaviour n is greater than 1 and there is a continuous change between stress and strain rate denoted by changing values of the

effective viscosity. According to Twiss and Moores (1992) and Ahrens (1995), rheological behaviour under low, moderate and high stress levels can be differentiated based upon the value of the exponent n (which in the first case are slightly larger but close to 1).

Talbot (1999) proposed a theoretical method to determine the value of the power law exponent (n) in the constitutive equation. The method considers the geometry of continuous passive markers deformed in shear zones (normally foliation traces) and compares it with the theoretical geometries that they would acquire when applying specific flow laws to the deformation of such markers. The method is prone to a certain degree of subjectivity during the process of drawing strain marker deflections (trajectories). Mulchrone (2001) developed a quantitative method to facilitate the calculation of n values and their error intervals. The physical basis of the mathematical formulation has been discussed by some authors (Fletcher, 2001; Sonder, 2001) who emphasized the influence of some variables (water fugacity and grain size, principally) that might result in variations of the effective viscosity of materials.

Theoretical trajectories calculated using Talbot's model and those observed in natural examples, such as those presented in Fig. 10, are very similar. This can be observed in a wide variety of rocks of different ages that were deformed in a different tectonic settings and over a range magnitude scales (Talbot, 1999). This strongly suggests that the influence of deformation mechanisms at the mineral lattice scale (or variations in grain size and water content) lead only to small deviations from the ideal geometrical pattern.

According to Talbot (1999), the portion of rock between the boundary and shear zone centre (i.e. half of the shear zone, of width w) exhibits a relationship between the displacement parallel to the shear zone (u) and the distance normal from the shear zone boundary (y) such that:

$$u/u_{\max} = 1 - (y/w)^{n+1} \tag{11}$$

where $u_{\max}$ is the maximum displacement along half the shear zone and n is related to the stress exponent of the constitutive equations.

A representative group of trajectories defined by the S1 foliation were taken from the drawings of the Bacariza Formation shear zones presented in Fig. 10a–e to determine a series of points (around 20) whose coordinates were taken with reference to the scheme presented in Fig. 12a. Following the mathematical procedure described by Mulchrone (2001), relevant values for the parameter n were calculated and are presented in Table 2. They range between 1.47 and 4.84 and reveal that the behaviour of the Bacariza granulite shear zones during D2 was dominantly plastic and that the stress regime was likely moderate.

Table 2
Values of the parameter n and error intervals calculated for the studied shear zones. The number of data is also included

Sample	n	Error	N. data
ZC1a	2.08	0.1	13
ZC1b	1.93	0.03	13
ZC3	3.31	0.15	16
ZC5b	1.86	0.04	7
ZC5c	3.06	0.15	11
ZC6a	3.02	0.1	17
ZC6b	1.64	0.26	21
ZC7a	1.47	0.03	18
ZC7b	4.84	0.35	20
ZC7c	2.27	0.01	20

6. Discussion and conclusions

As inferred from the geometrical and rheological analysis of shear zones from the Bacariza high-pressure granulite formation, these structures record negligible components of superimposed homogeneous deformation, flattening and volume change, and thus heterogeneous simple shear is thought to be the most important component of deformation. This was probably facilitated by a high competency contrast between the wall rocks and the material inside the shear zones. A detailed structural analysis of the shear zones enabled us to distinguish various influences on deformation patterns such as the effect that alternating lithologies had on shear zone geometry and the role of deformation localization leading to structural transposition of S1 fabrics by S2. Tectonic displacements in the shear zones were estimated to be of the order of hectometres to kilometres and were localized in a relatively thin portion of the Bacariza Formation near the basal thrust of overlying ultramafic massifs that were emplaced at temperatures of ca. 800 °C (Girardeau et al., 1989).

The study of these shear zones presents an apparent contradiction as regards (1) the plane strain heterogeneous simple shear model of deformation supported by most of our field observations and (2) the fact that structural sections of the shear zones normal to the movement direction exhibit fold structures that appear to indicate that, contrary to what was expected, shortening components also occurred in the direction normal to the plane XZ. The genetic and geometric models of sheath fold development proposed by Vollmer (1988) and Skjernaa (1989) are of primary importance in the context of this discussion. These authors showed that distortion of rock layers, initially containing smooth perturbations, could, in a plane strain simple shear deformation, lead to extreme amplification of such perturbations resulting in sheath and tubular folds. Sections across different parts of these structures exhibit eye-like (closed) and doubly-vergent (open) folds that in the absence of careful interpretation would appear to denote shortening in all directions normal to the sheath apical axis. If this genetic perspective is adopted, fold structures in sections normal to the lineation as observed in this study do not require a

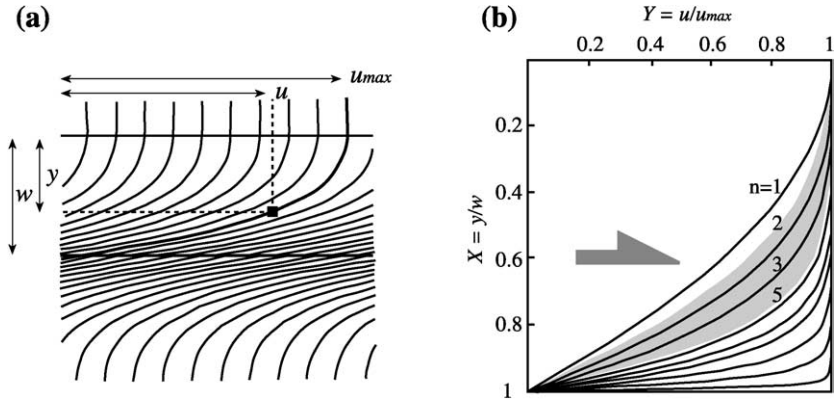

Fig. 12. (a) Geometry of a shear zone and nomenclature of the parameters used by Talbot (1999) to determine the exponent n-value of the flow laws. (b) Plot of the function $Y=1-X^{n+1}$ for different n-values. The arrow is parallel to the direction of the shear zone in (a) indicating its sense. Note that the geometry of some of these curves is quite similar to the trajectories of the real shear zone in (a). The shadowed area corresponds to the values calculated for the studied shear zones.

constrictional deformation regime and can readily develop in a plane strain simple shear regime. Although the initial presence of perturbations might indicate a component of shortening in all or some directions parallel to the foliation, the magnitude of this factor must be negligible in comparison with the magnitude of shear deformation.

Another question raised by this analysis is why high-temperature (and high-pressure) plastic deformation of crustal materials is so strongly localized instead of homogeneously distributed, in spite of the fact that the S1 fabric in the un-transposed wall rocks and the structurally transposed S2 fabric in the shear zone are both defined by the elongation of minerals of comparable metamorphic grade. We suggest that localization could relate to high strain rates associated with ultramafic nappe emplacement. The effect on deformation of high strain rates is comparable with that of contrasting temperatures in different parts of a rock volume. Work weakening within the shear zones could have produced an effect resembling localized ductile deformation in apparently harder blocks. Ábalos et al. (1996) described a similar mechanical effect in relation to paleopiezometric and effective viscosity determinations within a neighbouring Cabo Ortegal high-pressure nappe (the Concepenido eclogite massif) and its contact shear zones with the overlying Bacariza granulites. The fact that effective viscosities were larger in the shear zones (one order of magnitude) than within the eclogite massif (made of slightly higher-grade rocks) was related there to blocking of D1 rock ductile deformation within the eclogites as a result of effective viscosity increases (of various orders of magnitude) during cooling and to concomitant deformation localization into the bounding D2 shear zones. Effective viscosity in the latter would have increased during cooling also, but at a lower rate so that deformation localization was favoured.

The stress exponent calculated in this study for localized shear zone deformation under high temperatures and pressures points to a plastic rheological behaviour of granulites under moderate stress levels (20–60 MPa). This is in agreement with the results obtained in other high-pressure units of Cabo Ortegal (Ábalos et al., 1996; Gil Ibarguchi et al., 1999). Shear zones in gneisses and metasediments of comparable metamorphic grade yielded n-values >2.5, whereas low-grade sedimentary rocks yielded values close to 1 (viscous rheological behaviour; cf. Mulchrone, 2001). Various experimental and field studies of rock deformation in high-pressure settings performed in recent times (e.g. Stöckhert et al., 1997, 1999; Gerya and Stöckhert, 2002) have shown that this kind of rheological behaviour should be considered more as the rule than the exception in deep parts of orogenic convergence zones.

Acknowledgements

This study was financially supported by grants from the DGI-MCyT (BTE2001-0071 and BTE2002-03823) to P.P., B.A. and J.I.G.I. We gratefully acknowledge Dr J. Carreras for valuable comments and discussions on an early version of this paper and Drs B. Lafrance and F. Neubauer for their helpful reviews.

References

Ábalos, B., Azcárraga, J., Gil Ibarguchi, J.I., Mendia, M.S., Santos Zalduegui, J.F., 1996. Flow stress, strain rate and effective viscosity evaluation in a high-pressure nappe (Cabo Ortegal, Spain). Journal of Metamorphic Geology 14, 227–248.

Ábalos, B., Azcárraga, J., Gil Ibarguchi, J.I., Mendia, M.S., Puelles, P., 2000. Mapa Geológico del Complejo de Cabo Ortegal (NO de España). Instituto Universitario de Xeoloxía Isidro Parga Pondal, scale 1:42,750.

Ábalos, B., Puelles, P., Gil Ibarguchi, J.J., 2003. Structural assemblage of high-pressure mantle and crustal rocks in a subduction channel (Cabo Ortegal, NW Spain). Tectonics 22 (1), 1006.

Ahrens, T., 1995. Handbook of Physical Constants, vol. 3. American Geophysical Union, Washington, DC.

Alsop, G.I., 1992. Progressive deformation and the rotation of contemporary fold axes in the Ballybofey Nappe, northwest Ireland. Geological Journal 27, 271–283.

Arbaret, L., Mancktelow, N.S., Burg, J.P., 2001. Effect of shape and orientation on rigid particle rotation and matrix deformation in simple shear flow. Journal of Structural Geology 23, 113–125.

Beach, A., 1976. The interrelations of fluid transport, deformation, geochemistry and heat flow in early Proterozoic shear zones in the Lewisian complex. Philosophical Transactions Royal Society London A280, 569–604.

Bhattacharyya, P., Hudleston, P., 2001. Strain in ductile shear zones in the Caledonides of northern Sweden: a three-dimensional puzzle. Journal of Structural Geology 23, 1549–1565.

Carreras, J., 2001. Zooming on Northern Cap de Creus shear zones. Journal of Structural Geology 23, 1457–1486.

Carreras, J., García-Celma, A., 1982. Quartz c-axis fabric variation at the margins of a shear zone developed in schists from Cap de Creus (Spain). Acta Geológica Hispánica 17, 137–149.

Carreras, J., Estrada, A., White, S., 1977. The effects of folding on the *c*-axis fabric of a quartz-mylonite. Tectonophysics 39, 3–24.

Dale, J., Holland, T., Powell, R., 2000. Hornblende–garnet–plagioclase thermobarometry: a natural assemblage calibration of the thermodynamics of hornblende. Contributions to Mineralogy and Petrology 140, 353–362.

Dallmeyer, R.D., Martínez Catalán, J.R., Arenas, R., Gil Ibarguchi, J.I., Gutiérrez Alonso, G., Farias, P., Bastida, F., Aller, J., 1997. Diachronous variscan tectonothermal activity in the NW Iberian Massif: evidence from $^{40}Ar/^{39}Ar$ dating of regional fabrics. Tectonophysics 277, 307–337.

Droop, G.T.R., 1987. A general equation for estimating Fe^{3+} concentrations in ferromagnesian silicates and oxides from microprobe analyses using stoichiometric criteria. Mineralogical Magazine 51, 431–435.

Fletcher, R., 2001. Ductile shear zones as counterflow boundaries in pseudoplastic fluids. Journal of Structural Geology 23, 155–156.

Flinn, D., 1962. On folding during three-dimensional progressive deformation. Quaternary Journal of the Geological Society London 118, 385–428.

Galán, G., Marcos, A., 1997. Geochemical evolution of the high-pressure mafic granulites from the Bacariza formation (Cabo Ortegal complex, NW Spain): an example of a heterogeneous lower crust. Geologische Rundschau 86, 539–555.

Galán, G., Marcos, A., 2000. The metamorphic evolution of the high-pressure mafic granulites of the Bacariza Formation (Cabo Ortegal Complex, Hercynian belt, NW Spain). Lithos 54, 139–171.

Gapais, D., Balé, P., Choukroune, P., Cobbold, P.R., Mahjoub, Y., Mand, D., 1987. Bulk kinematics from shear zone patterns: some field examples. Journal of Structural Geology 9, 635–646.

Gerya, T.V., Stöckhert, B., 2001G. Exhumation rates of high-pressure metamorphic rocks in subduction channels: the effect of rheology. Geophysical Research Letters 29 (8), 102.

Ghosh, S.K., 1987. Measure of non-coaxiality. Journal of Structural Geology 9, 111–113.

Ghosh, S.K., Sengupta, S., 1987. Progressive development of structures in a ductile shear zone. Journal of Structural Geology 9, 277–287.

Gil Ibarguchi, I., Ábalos, B., Campillo, A., Higuero, A., López, B., Pinilla, V., Rodríguez, C., Rodríguez, R., Urtiaga, K., 1987. Asociaciones con granate-clinopiroxeno en la unidad catazonal superior del complejo de Cabo Ortegal. Cuadernos del Laboratorio Xeolóxico de Laxe 12, 165–181.

Gil Ibarguchi, J.I., Mendia, M., Girardeau, J., Peucat, J.J., 1990. Petrology of eclogites and clinopyroxene–garnet metabasites from the Cabo Ortegal Complex (northwestern Spain). Lithos 25, 133–162.

Gil Ibarguchi, J.I., Ábalos, B., Azcárraga, J., Puelles, P., 1999. Deformation, high-pressure metamorphism and exhumation of ultramafites in a deep subduction/collision setting (Cabo Ortegal, NW Spain). Journal of Metamorphic Geology 17, 747–764.

Gil Ibarguchi, J.I., Ábalos, B., Azcárraga, J., Mendia, M., Puelles, P., 2000. A petrological and structural excursion through the high-grade/high-pressure allochthonous units of the Cabo Ortegal Complex (NW Spain). Basement Tectonics 15, Mid-Conference Field Trip Guide, International Basement Tectonics Associated, La Coruña, Spain.

Girardeau, J., Gil Ibarguchi, J.I., 1991. Pyroxenite-rich peridotites of the Cabo Ortegal Complex (Northwestern Spain): evidence for large-scale upper-mantle heterogeneity. Journal of Petrology, 135–154 (special Lherzolites Issue).

Girardeau, J., Gil Ibarguchi, J.I., BenJamaa, N., 1989. Evidence for a heterogeneous upper mantle in the Cabo Ortegal Complex, Spain. Science 245, 1231–1233.

Hansen, E., 1971. Strain Facies. Springer, Berlin.

Harris, J., 1977. Rheology and Non-Newtonian Flow. Longman, London.

Hossack, J.R., 1968. Pebble deformation and thrusting in the Bygdin area (southern Norway). Tectonophysics 5, 315–339.

Hudleston, P.J., Schwerdtner, W.M., 1997. Strain. In: De Wit, M., Ashwal, L.D. (Eds.), Greenstone Belts. Oxford University Press, London, pp. 296–308.

Jaeger, J.C., 1969. Elasticity, Fracture and Flow. Wiley, New York.

Jain, A.K., 1988. Deformational and strain patterns of intracontinental collision ductile shear zones: example from Garwall Himalaya. Journal of Structural Geology 10, 717–734.

Mandal, N., Chakraborty, C., Samanta, S.K., 2001. Flattening in shear zones under constant volume: a theoretical evaluation. Journal of Structural Geology 23, 1771–1780.

Mandal, N., Chakraborty, C., Samanta, S.K., 2004. Reply to the comment by K. Mulchrone on: "Flattening in shear zones under constant volume: a theoretical evaluation" by N. Mandal, C. Chakraborty and S. Samanta. Journal of Structural Geology 26, 197–200.

Martínez Catalán, J.R., Arenas, R., Díaz García, F., Abati, J., 1997. Variscan accretionary complex of northwest Iberia: Terrane correlation and succession of tectonothermal events. Geology 25, 1103–1106.

Means, W.D., 1990. Kinematics, stress, deformation and material behavior. Journal of Structural Geology 12, 953–971.

Mohanty, S., Ramsay, J.G., 1994. Strain partitioning in ductile shear zones: an example from a lower pennine nappe of Switzerland. Journal of Structural Geology 16, 663–676.

Mulchrone, K.F., 2001. Quantitative estimation of exponents of power-law flow with confidence intervals in ductile shear zones. Journal of Structural Geology 23, 803–806.

Mulchrone, K.F., 2004. Discussion on "Flattening in shear zones under constant volume: a theoretical evaluation" by N. Mandal, C. Chakraborty and S. Samanta. Journal of Structural Geology 26, 201–202.

Nicolas, A., Poirier, J.P., 1976. Crystalline Plasticity and Solid-state Flow in Metamorphic Rocks. Wiley, New York.

Ordóñez, B., Gebauer, D., Schäfer, H.-J., Gil Ibarguchi, J.I., Peucat, J.J., 2001. A single Devonian subduction event for the HP/HT metamorphism of the Cabo Ortegal Complex within the Iberian Massif. Tectonophysics 232, 359–385.

Peucat, J.J., Bernard-Griffiths, J., Gil Ibarguchi, J.I., Dallmeyer, R.D., Menot, R.P., Cornichet, J., Iglesias Ponce de León, M., 1990. Geochemical and geochronological cross section of the deep Variscan crust: the Cabo Ortegal high-pressure nappe (NW Spain). Tectonophysics 177, 263–292.

Puelles, P., 2004. Deformación, metamorfismo y exhumación de las granulitas de alta presión de la Bacariza (Complejo de Cabo Ortegal, NO de España). Nova Terra 23, La Coruña, Spain.

Puelles, P., Ábalos, B., Gil Ibarguchi, J.I., 2001. Rasgos estructurales de la formación granulítica de alta presión de la Bacariza (Cabo Ortegal, NO España). Geogaceta 30, 115–118.

Puelles, P., Ábalos, B., Gil Ibarguchi, J.I. 2005. Metamorphic evolution and thermobaric structure of the subduction-related Bacariza high-pressure granulite formation (Cabo Ortegal Complex, NW Spain). Lithos, d.o.i.: 10.1016/j.lithos.2005.01.009.

Ramsay, J.G., 1967. Folding and Fracturing of Rocks. McGraw-Hill, New York.

Ramsay, J.G., 1980. Shear zone geometry: a review. Journal of Structural Geology 2, 83–89.

Ramsay, J.G., Graham, R.H., 1970. Strain variations in shear belts. Canadian Journal of Earth Sciences 7, 786–813.

Ramsay, J.G., Huber, M.I., 1983. The Techniques of Modern Structural Geology, Strain Analysis, vol. 1. Academic Press, London.

Ramsay, J.G., Huber, M.I., 1987. The Techniques of Modern Structural Geology, Folds and Fractures, vol. 2. Academic Press, London.

Ramsay, J.G., Lisle, R.J., 2000. The Techniques of Modern Structural Geology, Applications of Continuum Mechanics in Structural Geology, vol. 3. Academic Press, London.

Ries, A., Shackleton, R.M., 1971. Catazonal complexes of north-western Spain and north Portugal; remnants of a Hercynian thrust plate. Natural and Physical Science 234, 65–69.

Ring, U., 1998. Volume strain, strain type and flow path in a narrow shear zone. Geologische Rundschau 86, 786–801.

Ring, U., 1999. Volume loss, fluid flow, and coaxial versus noncoaxial deformation in retrograde, amphibolite facies shear zones, northern Malawi, eastern-central Africa. Geological Society of America Bulletin 111, 123–142.

Santos Zalduegui, J.F., Schärer, U., Gil Ibarguchi, J.I., 1996. Isotope constraints on the age and origin of magmatism and metamorphism in the Malpica-Tuy Allochthon. Chemical Geology 121, 91–103.

Santos Zalduegui, J.F., Schärer, U., GilI barguchi, J.I., Girardeau, J., 2002. Genesis of pyroxenite-rich peridotite at Cabo Ortegal (NW Spain): geochemical and Pb–Sr–Nd isotope data. Journal of Petrology 43, 17–43.

Skjernaa, L., 1989. Tubular folds and sheath folds: definitions and conceptual models for their development, with examples from the Grapesvare area, northern Sweden. Journal of Structural Geology 11, 689–703.

Sonder, L., 2001. Ductile shear zones as counterflow boundaries in pseudoplastic fluids: discussion and theory. Journal of Structural Geology 23, 151–155.

Stöckhert, B., Massone, H.-J., Nowlan, E.U., 1997. Low differential stress during high-pressure metamorphism: the microstructural record of a metapelite of the Eclogite Zone, Tauern Window, Eastern Alps. Lithos 41, 103–118.

Stöckhert, B., Brix, M.R., Kleinschrodt, R., Hurford, A.J., Wirth, R., 1999. Thermochronology and microstructures of quartz-a comparison with experimental flow laws and predictions on the temperature of the brittle-plastic transition. Journal of Structural Geology 21, 351–369.

Sturm, R., 2003. SHEARCALC—a computer program for the calculation of volume change and mass transfer in a ductile shear zone. Computers & Geosciences 29, 961–969.

Talbot, C.J., 1999. Ductile shear zones as counterflow boundaries in pseudoplastic fluids. Journal of Structural Geology 21, 1535–1551.

Tikoff, B., Fossen, H., 1999. Three-dimensional reference deformations and strain facies. Journal of Structural Geology 21, 1497–1512.

Twiss, R.J., Moores, E.M., 1992. Structural Geology. Freeman and Co, New York.

Valín, M.L., Pérez-Estaun, A., Martín-Izard, A., Marcos, A., 1994. Variación de la textura y química mineral de rocas metabásicas en una zona de cizalla (Complejo de Cabo Ortegal, NW de España). Revista de la Sociedad Geológica de España 7, 179–189.

Van Calsteren, P.W.C., Boelrijk, N.A.I.M., Hebeda, E.H., Priem, H.N.A., Den Tex, E., Verdurmen, E.A.T., Verschure, R.H., 1979. Isotopic dating of older elements (including the Cabo Ortegal mafic-ultramafic complex) in the Hercynian orogen of NW Spain: manifestations of a presumed early Palaeozoic mantle-plume. Chemical Geology 24, 35–56.

Vogel, D.E., 1967. Petrology of eclogite- and pyrigarnite-bearing polymetamorphic rock complex at Cabo Ortegal, NW Spain. Leidse Geologische Mededelingen 40, 121–213.

Vollmer, F.W., 1988. A computer model of sheath-nappes formed during crustal shear in the Western Gneiss Region, central Norwegian Caledonides. Journal of Structural Geology 10, 735–743.